Journal of Ceramic Processing Research. Vol. 21, No. 4, pp. 501~507 (2020)
(Received 4 March 2020, Received in revised form 23 March 2020, Accepted 24 March 2020)
https://doi.org/10.36410/jcpr.2020.21.4.501

J O U R N A L O F
Ceramic Processing Research

Ballistic study of alumina ceramic-steel composite for structural applications

Olawale M. Sanusi[a,b,*], Olatunde A. Oyelaran[b] and Jubril A. Badmus[b]
[a]*INSA Centre Val de Loire, Laboratoire de Mécanique Gabriel Lamé (LaMé), Blois, France*
[b]*Mechanical Engineering Department, Federal University Oye-Ekiti, Ekiti, Nigeria*

The protection of security/military personnel and their structural facilities such as vehicles, aircraft and other security hardware continues to attract research attention as trade-off between weight and protection lingers. Ceramics are employed in lightweight armour system for its ballistic efficiency and weight advantage; meanwhile, it is comparatively expensive. This research examined the effectiveness of sintered alumina, developed from corundum, as a laminate component of ceramic-steel composite for structural armour applications. Both armour steel and medium carbon steel were separately impacted by 7.62 × 51 mm armour-piercing (AP) projectile before laminated with the prepared sintered ceramic in evaluating its ballistic resistance. The mechanical properties of the sintered ceramic compete favourably with the commercial CoorsTEK® sintered ceramics. Subsequently, varying target configurations of the ceramic and medium carbon steel composites were studied and analyzed against the same projectile in accordance with NIJ Standard-0108.01. The composite structure, depending on the configuration, displays different forms of failure modes. The high-impact experimental study confirmed the protective capability of the sintered ceramic by its severity interaction against projectile and delay of projectile penetration when used as a laminate component plate.

Keywords: Armour, Alumina ceramics, Ammunition, Composite, Corundum.

Introduction

Armour is a shield provided for ballistic defeat of projectiles or blast fragment when integral protection of a coverage area is insufficient [1]. Armours are made from metallic plates [2], ceramics, compressed laminate sheets or composites that incorporate two or more of these materials for ballistic resistance effectiveness at comparatively low weight [3-5]. Ali *et al*. [6] reported a complete perforation of 20 mm thick aluminium armoured plate, while its combination with perforated armoured steel was able to stop 7.62 mm projectile. Conventionally, vehicular ballistic protection is primarily made of high hardness steel [7] due to its maintenance of structural rigidity and strength [3]. Meanwhile, as majority of systems requiring projectile protection are mobile (military vehicle, tank, aircraft and military/ security personnel), weight becomes a critical parameter in armour design [8]. Secondly, ease of defeating strong steel by armour-piercing (AP) projectile, which carries a high hardness [2] and high kinetic energy penetrating core [9], is another challenge of steel. These necessitated a sustained quest for high performance, lightweight and cost-effective materials for personnel and vehicles to improve manoeuvrability, survivability and reduce injury when exposed to threats including blast [10, 11].

Ceramic/steel composites are therefore been lately integrated to offer more efficient lightweight armours [12-16]. For instance, Pawar *et al*. [17] compared the influence of Al_2O_3 or AlN ceramics over the deformation pattern of metallic backing plate. They found that AlN ceramic created less bulging on the backing plate compared to Al_2O_3 due to AlN higher shear strength that suppressed the wing crack formation on application of compressive load. They opined that the backing deformation is dependent on the ceramic chemical composition. Jinzhu *et al*. [16] investigated the penetration of tungsten alloy rod into alumina/ armour steel composite. They found that the penetration depth decreased with the ceramic thickness and that the ceramic was comminuted on impact spot, which made it to split into small fragment sizes determined by the distance from the impact spot. Another study on layers of ceramic/metallic backing [18] reported a better ballistic effect when the ceramic was aligned in an oblique position against impending projectile. Nevertheless, the relevance of interfacial interaction and different structural configurations of components that give optimum ballistic efficiency requires more focus [19].

In the bi-layer ceramic/steel system, the ceramic component (due to its high hardness and compression strength [12, 20]) causes blunt and fracture of the core of armour-piercing projectile, thereby reducing the projectile penetrating power [21]. Complementarily, the backing steel absorbs the kinetic energy of the retarded blunt-projectile as well as retaining the fragments from

*Corresponding author:
Tel : +33602120550
E-mail: olawale.sanusi@insa-cvl.fr; olawalem.sanusi@fuoye.edu.ng

both ceramic and projectile hindering the fragments from causing further harm [22]. Specifically, low density, high rigidity and compression strength make ceramics effective [12, 20] and suitable for armour systems protection; including aircraft structures and military vehicles [23-26]. Besides the ceramic counter-interaction with high-kinetic energy weapons (from small calibres up to medium armour piercing calibres or higher [27, 28]), it offers a weight advantage of 2-3 times less than its steel equivalent [29]. Several ceramic materials are used in bi-layer ballistic armours including alumina [30-32], boron carbide (B_4C) [33], silicon carbide (SiC) [29]. However, this advanced ceramics component of armour system are generally very expensive and challenging in terms of processing and shaping as it requires both high temperature and pressure [27, 34].

Off all the advanced ceramics for armour, alumina is relatively cheap with exceptionally high hardness and exhibits unique compact crystal structure [8]. Aside from its exceptional chemical and fire resistance, alumina ceramic high wear and deformation resistance [35] provides excellent resistance to projectile. The most important raw material for the production of alumina is bauxite, which is a mixture of the minerals boehmite (α-AlO(OH)), diaspor (β-AlO(OH)), and gibbsite ($Al(OH)_3$), with a high content of various impurities such as Na_2O, SiO_2, TiO_2, and Fe_2O_3. Bauxite is refined using the Bayer process that requires hot sodium hydroxide solution with high pressure [36] while very pure commercial powders are prepared via the calcination of alum, $NH_4Al(SO_4)_2$-$12H_2O$ [37, 38]; these are purely thermal process. Sol-gel method also produces high-purity alumina, but its industrial operation is too costly and requires the use of highly pollutant solutions [39-41].

Alumina occurs naturally as corundum (igneous and metamorphic rocks) and could serve as a substitute to other sources of alumina for advanced ceramics. Interestingly, corundum purification through froth floatation method does not require corrosive and thermal processing for conversion to pure alumina [42-44]. In this work, the influence of sintered alumina, prepared from froth-floatation of corundum, was investigated for the first time as a laminate in ceramic/steel composite armour system. The ceramic ballistic potency was studied against armour piercing projectile, while used as laminate with both armour steel and ordinary commercial medium-carbon-steel, for structural armour applications.

Experimental

Materials

Alumina powder, prepared via froth floatation of corundum [43, 45], was used as ceramic matrix. Briefly, corundum granulates was measured into a floatation cell containing ionized water and then agitated at 2000 rev/min. The pH of the solution was maintained around 2.5 – 3 prior to addition of petroleum sulphate and hydrofluoric acid, which served as corundum collector and activator, respectively. Compressed air was then introduced into the solution to create bubbles within the continuously agitated solution and consequently led to the floatation of alumina while other compounds depressed. The floated alumina was collected, washed and dried; thereafter, the process was repeated three times before the optimum alumina content, determined by Phillips 1404 XRF X-ray fluorescence spectrometer, was attained (Table 1). Other materials were used as-received: Polyvinyl alcohol (PVA) and calcium oxide (CaO) (Sigma-Aldrich, UK); magnesium oxide (MgO) (Tateho, Japan). Armour steel and commercial medium carbon steel (donated by Defence Industries Corporation of Nigeria; DICON) were separately used as backing steels. The armour steel and commercial medium steel (Delta Steel, Nigeria) chemical composition and mechanical properties are given in Tables 2 and 3 as determined [46] and specified by the manufacturer, respectively. The ammunition used was 7.62 × 51 mm armour-piercing (AP) manufactured by DICON.

Preparation of alumina ceramic

The dried alumina powder, PVA, CaO and MgO were weighted in 95.66, 2.78, 1.28 and 0.28 %wt, respectively, the optimum material elaboration ratio is determined from the previous work [47]. The composition was thoroughly mixed to form free flowing dry powder, which was transferred into metallic mould (100 × 100 × 20 mm) and compacted uniaxially under 110 MPa. After that, the pressed sample was sintered (Brother Furnace XD-1700M) at 1500 °C for 60 min; Fig. 1.

Table 1. Chemical composition of the froth floated alumina powder

Compound	Al_2O_3	SiO_2	Fe_2O_3	TiO_2	CaO	P_2O_5
(Wt.%)	86.600	5.900	3.575	0.949	0.323	0.400

Table 2. Chemical compositions of armour steel and medium carbon steel

	C	Mn	Si	Ni	Co	Cr	Mo	Nb	V	Ti	B	P	S	Fe
A	0.25	0.98	0.18	0.04	2.35	1.2	0.5	0.08	0.08	0.06	0.01	0.01	0.01	Bal.
C	0.33	0.78	0.16	0.09	0.01	0.1	0.11	0.01*	0.002	0.01	0.04	0.05	0.04	Bal.

NB: ***A*** means **armour steel**; and ***C*** means **commercial medium carbon steel**; *Pb

Table 3. Mechanical properties of amour steel and medium carbon steel

	Tensile strength (MPa)	Impact energy (J)	Elongation (%)	Hardness (BHN)
A	1290	27	10.1	483
C	946	42	25	269

Fig. 1. (a) Mould assembly; (b) green sample extracted from the mould; (c) sintered ceramics samples.

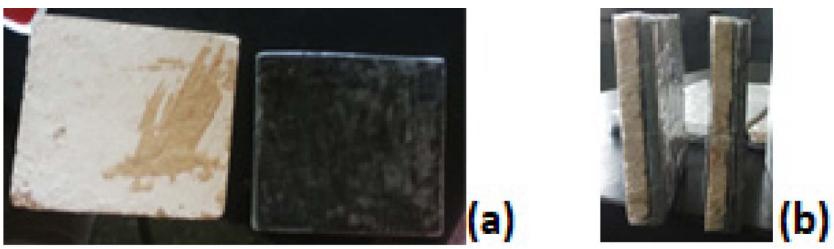

Fig. 2. (a) sintered ceramic (left) and backing steel (right); (b) assembled composite.

Density, ρ, compressive strength, *CCS*, (ASTM C773-88), flexural strength, σ_{fs}, (ASTM C1161-94), modulus of elasticity, *E*, (ASTM-C848) and fracture toughness, K_{IC}, (ASTM C1421-10) of the sintered alumina was determined from Eq. 1-5 [48], respectively. Hardness (ASTM C1421) with N-scale diamond cone indenter was determined on Rockwell hardness tester (Mitutoyo AKT-6).

$$\rho = \frac{M}{V} \tag{1}$$

Where, *M* and *V* are mass and volume of the ceramic, respectively.

$$CCS = \frac{F}{A} \tag{2}$$

Where, *F* is maximum force; *A* is normal area to the applied force, *A* = w * b

$$\sigma_{fs} - \frac{3FL}{2bh^2} \tag{3}$$

$$E = \frac{L^3 F}{4bh^3 \delta} \tag{4}$$

Where, *L, b* and *h* are span length, width and height respectively.

$$K_{IC} = \frac{FL}{bh^{\frac{3}{2}}}\left\{2.9\left(\frac{a}{h}\right)^{\frac{1}{2}} - 4.6\left(\frac{a}{h}\right)^{\frac{3}{2}} + 21.8\left(\frac{a}{h}\right)^{\frac{5}{2}} - 37.6\left(\frac{a}{h}\right)^{\frac{7}{2}} + 38.7\left(\frac{a}{h}\right)^{\frac{9}{2}}\right\} \tag{5}$$

Where, *a* is crack length measured after fracture; for Eq. 5, *L* = 8*b*; *h* = 2*b*.

Preparation of ceramic-steel laminate

The 6 mm-thick backing (armour steel and medium carbon steel) used for this research was cut into 100 × 100 mm in order to match the prepared 8 mm-thick sintered alumina ceramic; Fig. 2(a). Subsequently, the sintered ceramic was glued on to the surface of the prepared backing steel using synthetic Araldlte® epoxy adhesive and then left to dry for 24 hours at 26 MPa. Thereafter, the glued plates were wrapped with transparent polypropylene in order to enhance the firmness; Fig. 2(b).

Ballistic evaluation

The prepared samples were first conditioned at 23 ºC for 24 hrs [49-51]. The weapon was set, levelled and positioned on the gun mount, Fig. 3(a). All tests were taken at normal obliquity and 15 m from the weapon muzzle. The projectile velocity was maintained at 838

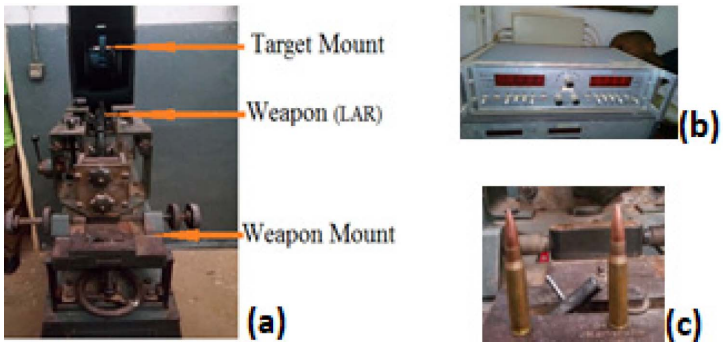

Fig. 3. (a) Ballistic test setup at DICON (b) chronograph (c) 7.62 × 51 mm ammunitions.

Table 4. Mechanical properties of sintered ceramic

	ρ (g/cm^3)	CS (MPa)	FS (MPa)	E (GPa)	K_{IC} (MPa.m$^{1/2}$)	BHN
AC-86.6	**3.45**	**1912**	**295**	**270**	**3.75**	**75**
AD-85	3.42	1930	296	221	3-4	73
AD-90	3.60	2482	338	276	3-4	75
AD-995	3.90	2600	379	370	4-5	83

NB: Value after the hyphenated letter is the Al_2O_3 % of the alumina, e.g. **AC-86.6;** AD [53]

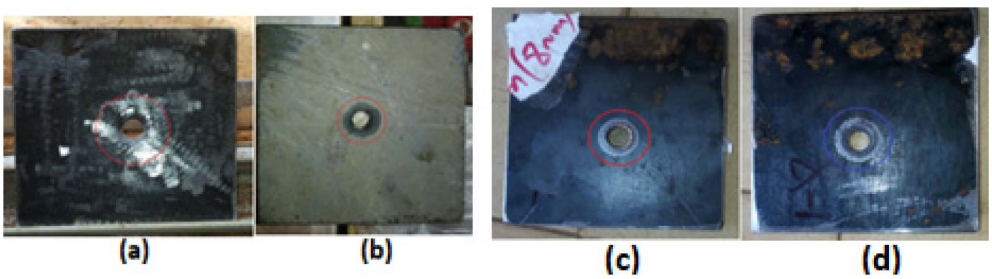

Fig. 4. (a) Front; (b) back view of armour steel; (c) Front; (d) back view of medium carbon steel with complete perforation.

± 15 m/s. Light automatic rifle (LAR) was used for firing the 7.62 × 51 AP ammunition; Fig. 3(b, c).

Results and Discussion

Physical properties of the sintered alumina

AD-series ceramic, one of the most reported commercial alumina used in literature for ceramic armour [48, 52], is compared with our alumina ceramics developed from corundum. Table 4 shows the comparative physical properties of the sintered alumina (**AC-86.6**) and commercial CoorsTEK® (AD-series, Al_2O_3%) ceramics [53]. The properties of the sintered alumina ceramic were found to be comparable with the values of AD-series, which suggests its efficacy for armour applications.

Ballistic evaluation result

Monolithic backing steel: armour and medium carbon steel (*S*)

Armour steel was first evaluated against 7.62 × 51 mm AP. The result of the impact against the as-received armour steel plate at 0° obliquity is depicted in Fig. 4a (front) and 4b (rear). The plate was penetrated completely through rearward petalling mode of perforation failure. This was expected as the strongest steel could easily be defeated by AP projectile [54]. The plate slightly bent inward at the impact of the projectile which induced large circumferential stress at the impact point, and the compressive wave propagated inward which led to the failure of the armour steel [55]. The reverse side of the armour plate showed minute ductile hole enlargement deformation, which is comparable to past literature [56]. Similarly, at the impact of the low medium steel, the sample failed by exhibiting petalling failure mode but with an associated hole enlargement in both the front and back faces of the steel (Fig. 4(c-d)). This failure mode is typically observed in a high ductile metal in which the nose of the conical bullet concentrated stresses at the contact point and resulted in intense deformation of the crater axis [57, 58]. Therefore, irrespective of the steel type, that is the armour and the ordinary medium carbon steel, the ammunition could penetrate the sample steels.

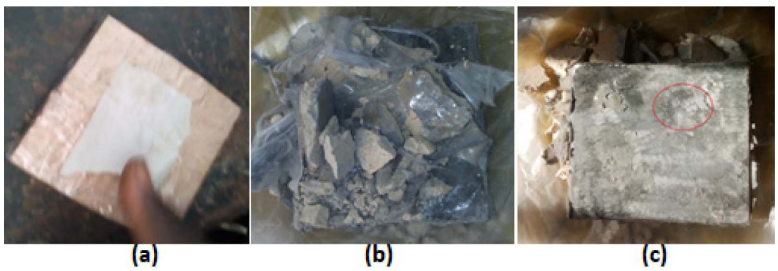

Fig. 5. (a) Laminate of ceramic and the Steel before impact (b) Fractured ceramic of the composite sample against the bullet impact; (c) Impression of the bullet impact on armour plate (red circle) after ceramic fracture.

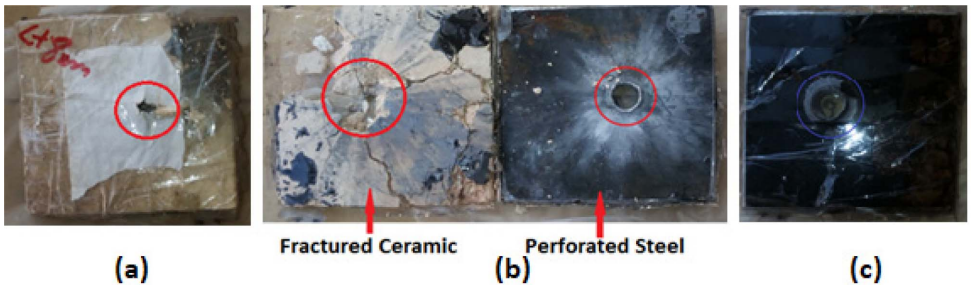

Fig. 6. (a) Perforated composite sample; (b) separated ceramic and steel after impact; (c) backside of the armour assembly (projectile exit).

Different configurations of sintered alumina and steel

Laminate of sintered alumina-steel (*C*-S)

The efficacy of the developed ceramic was first determined by placing it over the monolithic armour and medium carbon steel separately to form bilayer composites. The laminate of ceramic and armour steel before and after bullet impact are shown in Fig. 5(a) and Fig. 5(b), respectively. The frontal ceramic debonded and failed by pulverization into several pieces; while the backing armour steel was intact after the projectile impact. The ceramic, supported by high strength armour steel, significantly interacted with the projectile and lowered its energy, which resulted in the protection of the armour steel with less bulge on it, Fig. 5(c). As remarkably observed in [15], bi-layered structure of metal/ceramic showed better ballistic performance because the ceramic eroded the bullet through cracking while the metal absorbed the remnant projectile kinetic energy by its deformation.

However, the laminate of ceramic and medium steel could not stop the penetration. Fig. 6(a) (red circle) shows the penetrated assembly of ceramic/medium steel after impact. The penetrated assembly was separated to reveal the damage mode in the two components; Fig. 6(b). The ceramic displays radial crack fracture mode while the steel showed less but melted petals deformation and insignificant bending of the steel plate as a result of reduced stress brought about by the fractured frontal alumina, compared to monolithic medium steel. The fractured ceramic formed conoids that distributed the projectile energy and resulted in lower energy on the medium steel; however, low strength and hardness of the steel could not resist the bullet penetration. The low resistance offered by the medium steel caused reduced lateral wave rarefaction reflected from the ceramic-steel boundary [16]. Thus, a radial cracking of the ceramic was observed unlike the crumbled ceramic nature observed in the ceramic-armour steel because of more resistance offered by high strength armour steel. The projectile exit point (steel rear side) produced ductile hole enlargement failure mode; Fig. 6(c).

Laminate of steel-sintered ceramic-steel (S-*C*-S)

After the failure of the ceramic/medium carbon steel assembly, the ceramic was then sandwiched in between two medium-carbon steels (Fig. 7a) and evaluated. The impacted assembly (Fig. 7b) had its frontal steel perforated with conspicuous outward petalling mode of failure. This failure mode confirmed the delay in projectile penetration as a result of enormous circumferential stress developed through the medium steel thickness [59] orchestrated by high resistance posed by the ceramic. On separation of the components (Fig. 7c), it was observed that the **S-*C*-S** assembly successfully stopped the bullet; after penetrating the first steel plate and fractured the ceramic; this is termed partial penetration. Radial fracture of the ceramic is apparent because of intense projectile-ceramic interaction. The yellow circle on Fig. 7c signifies point of bullet impact on the second steel before exiting the assembly with some fractured ceramic. The blue circle on Fig. 7d depicts the impact impression (bulge) left on the backing steel (second) after the assembly successfully stopped

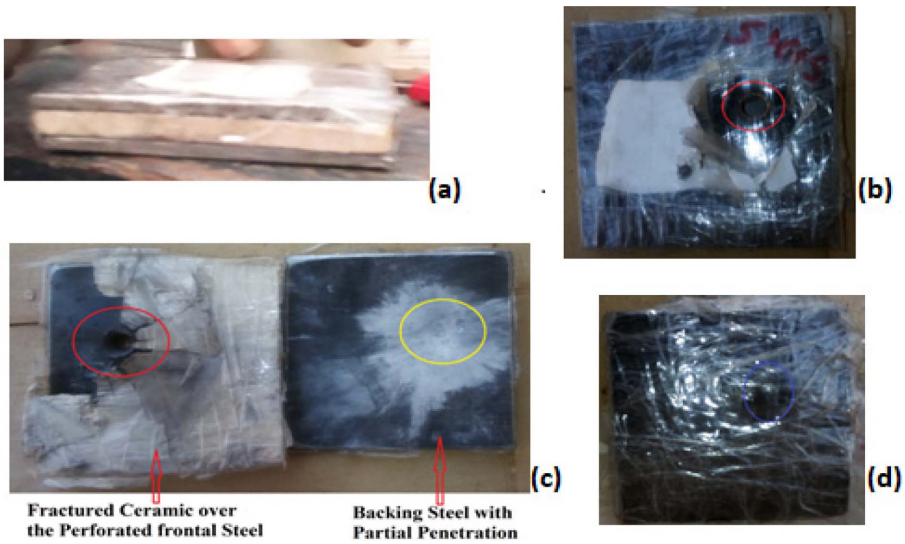

Fig. 7. (a) **S-*C*-S** before; (b) after impact; (c) separated backing steel from the armour system after impact; (d) bulging of the backing steel (blue circle).

the projectile. This result is in agreement with literature [60] that reported that the ballistic performance increased with increased cover plate thickness.

Conclusion

This research studied the effectiveness of sintered alumina, developed from corundum, as a laminate component of ceramic-steel composite for structural applications. The sintered ceramic displayed competitive mechanical properties that serve as an alternative to the commercial sintered ceramics for armour applications. The ballistic study revealed protective capability of the sintered ceramic by its severity interaction against projectile and delay of projectile penetration when used as laminate component. First, the ceramic effectively shielded armour steel. Secondly, a functional laminate configuration, steel-ceramic-steel (S-*C*-S), was found to be effective in arresting impending AP with ordinary commercial medium-carbon-steel. Finally, the ballistic performance of the composite would be greatly enhanced if the hardness of the medium carbon steel is improved by appropriate heat treatment.

Acknowledgements

Defence Industries Corporation of Nigeria (DICON) is appreciated for the use of her facilities and provision of steel materials for ballistic examination.

References

1. A. Serjouei, R. Chi, Z. Zhang, and I. Sridhar, Int. J. Impact Eng. 77 (2015) 30-41.
2. B. Mishra, B. Ramakrishna, P.K. Jena, K. Siva Kumar, V. Madhu, and N.K. Gupta, Mater. Des. 43 (2013) 17-24.
3. S.H. Atapek and S. Karagoz, Def. Sci. J. 61[1] (2011) 81-87.
4. S. Feli and M.R. Asgari, Compos. Part B Eng. 42[4] (2011) 771-780.
5. R. Chi, A. Serjouei, I. Sridhar, and G.E.B. Tan, Int. J. Impact Eng. 52 (2013) 37-46.
6. M.W. Ali, A. Mubashar, E. Uddin, S.W.U. Haq, and M. Khan, Int. J. Impact Eng. 110 (2017) 47-56.
7. Z. Fawaz, W. Zheng, and K. Behdinan, Compos. Struct. 63[3-4] (2004) 387-395.
8. W. Liu, Z. Chen, X. Cheng, Y. Wang, A.R. Amankwa, and J. Xu, Compos. Part B Eng. 84 (2016) 33-40.
9. G. Di Benedetto, P. Matteis, and G. Scavino, Int. J. Impact Eng. 115 (2018) 10-18.
10. J.D. Clayton, Int. J. Impact Eng. 85 (2015) 124-131.
11. K. Amini, W. Altenhof, S.C.K. Yuen, C.J. Opperman, and G.N. Nurick, Int. J. Impact Eng. 110 (2017) 228-241.
12. R. Yi, L. Yin, J. Wang, Z. Chen, and D. Hu, Def. Technol. 13[4] (2017) 295-299.
13. E. Medvedovski, Ceram. Int. 36[7] (2010) 2117-2127.
14. K. Akella, Procedia Eng. 173 (2017) 244-250.
15. X. Guo, X. Sun, X. Tian, G.J. Weng, Q.D. Ouyang, and L.L. Zhu, Compos. Struct. 157 (2016) 163-173.
16. L. Jinzhu, Z. Liansheng, and H. Fenglei, Int. J. Impact Eng. 101 (2017) 1-8.
17. M.J. Pawar, A. Patnaik, S.K. Biswas, U. Pandel, I.K. Bhat, S. Chatterjee, A.K. Mukhopadhyay, R. Banerjee, B.P. Babu, Int. J. Impact Eng. 98 (2016) 42-51.
18. D. Luo, Y. Wang, F. Wang, H. Cheng, and Y. Zhu, Mater. 12[18] (2019) 2946.
19. J.D. Clayton, Math. Probl. Eng. 2015 (2015) 709498.
20. D. Hu, J. Wang, L. Yin, Z. Chen, R. Yi, and C. Lu, Def. Technol. 13 (2017) 281-287.
21. C. Evci and M. Gülgeç, J. Compos. Mater. 48[26] (2014) 3215-3236.
22. K. Krishnan, S. Sockalingam, S. Bansal, and S.D. Rajan, Compos. Part B Eng. 41[8] (2010) 583-593.
23. B. Tepeduzu and R. Karakuzu, Ceram. Int. 45[2] (2019) 1651-1660.
24. R. Chi, A. Serjouei, I. Sridhar, and T.E.B. Geoffrey, Int. J. Impact Eng. 84 (2015) 159-170.

25. Q. Wang, Z. Chen, and Z. Chen, Mater. Des. 46 (2013) 634-639.
26. M.V. Silva, D. Stainer, H.A. Al-Qureshi, O.R.K. Montedo, and D. Hotza, J. Ceram. 2014 (2014) 1-6.
27. I.G. Crouch, M. Kesharaju, and R. Nagarajah, Ceram. Int. 41[9] (2015) 11581-11591.
28. V.M. Castaño and R. Rodríguez, Mater. Technol. 47[3] (2013) 267-271.
29. M. Cegła, W. Habaj, W. Stępniak, and P. Podgorzak, Fibres Text. East. Eur. 1[109] (2015) 85-88.
30. J. Venkatesan, M.A. Iqbal, and V. Madhu, Procedia Eng. 173 (2017) 671-678.
31. A.Y. Badmos and D.G. Ivey, J. Mater. Sci. 36[20] (2001) 4995-5005.
32. E.G. Pickering, M.R. O'Masta, H.N.G. Wadley, and V.S. Deshpande, Int. J. Impact Eng. 110 (2017) 123-137.
33. S.G. Savio, K. Ramanjaneyulu, V. Madhu, and T.B. Bhat, Int. J. Impact Eng. 38[7] (2011) 535-541.
34. K. Akella and N.K. Naik, J. Indian Inst. Sci. 95[3] (2015) 297-312.
35. M. Lee and Y.H. Yoo, Int. J. Impact Eng. 25 (2001) 819-829.
36. D.S. Lima and O.W. Perez-Lopez, J. Therm. Anal. Calorim. 1 (2020) 1-12.
37. K. Davis, Sch. Dr. Stud. Eur. Union J. 2 (2010) 109-114.
38. A.A. Taromi and S. Kaliaguine, Microporous Mesoporous Mater. 248 (2017) 179-191.
39. A. Souto, A. Rodriguez, and F. Guitián, J. Eur. Ceram. Soc. 20[6] (2000) 695-698.
40. L. Wang, in Proceedings of 2nd International Conference on Materials Science and Nanotechnology, April 2017, edited by Z. Chen, T. Pasang, K. T. Lau, M. Zhu (ICMSNT Press, 2017) p.1-6.
41. G. Feng, F. Jiang, W. Jiang, J. Liu, Q. Zhang, Q. Hu, L. Miao, and Q. Wu, Ceram. Int. 45[1] (2019) 354-360.
42. C.W. Smith and T.O. Llewellyn, in "Pioneering studies on the flotation of corundum from a Montana gneiss" (USA: Bureau of Mines, 1987) p.1-4.
43. O.M. Sanusi, M. Dauda, A.S. Ahmed, M.T. Isa, J.O. Akindapo, O.A. Oyelaran, and T.O. Ogundana, Ife J. Technol. 25[1] (2018) 34-38.
44. M. Farahmandjou and N. Golabiyan, Mater. Eng. Res. 1[2] (2019). 40-44.
45. J.A. Kitchener, in "The Scientific Basis of Flotation, edited by K. J. Ives (Dordrecht: Springer, 1984) p.3-51.
46. O.M. Sanusi, J.O. Akindapo, M. Dauda, Y. Bello, and M.O. Olaleke, Ife J. Technol. 24[1] (2016) 1-5.
47. O.M. Sanusi, M. Dauda, M. Sumaila, A.S. Ahmed, M.T. Isa, O.A. Oyelaran, and O.O. Martins, Aceh Int. J. Sci. Technol. 7[1] (2018) 32-43.
48. J.J. Swab, J. Tice, A.A. Wereszczak, and R.H. Kraft, J. Am. Ceram. Soc. 98[2] (2015) 607-615.
49. NIJ Standard 0108.01, in "Ballistic Resistant Protective Materials" (National Institute of Justice, U.S. Department of Justice, 1985) p.1-9.
50. US Military Standard, No. MIL-STD-662F (1997) p.1-15.
51. A. Bhatnagar, in "Lightweight Ballistic Composites: Military and Law-Enforcement Applications" (Woodhead Publishing, 2016) p.115-156.
52. A. Serjouei, R. Chi, I. Sridhar, and G.E.B. Tan, Procedia Eng. 75 (2014) 14-18.
53. CoorsTek, in "Advanced alumina materials and manufacturing processes" (COORSTEK Brochures. USA, 2016) p.2.
54. J.R. Denzel, in "Determination of shock properties of ceramic corbit 98: 98% alumina" (Naval Postgraduate School, 2010) p.3.
55. Ş.H. Atapek, Def. Sci. J. 63[3] (2013) 271-277.
56. N. Kiliç and B. Ekici, Mater. Des. 44 (2013) 35-48.
57. T. Wierzbicki, Int. J. Impact Eng. 22[9-10] (1999) 935-954.
58. P.K. Jena, B. Mishra, K. Siva Kumar, and T.B. Bhat, Mater. Des. 31[7] (2010) 3308-3316.
59. T. Deniz, in "Ballistic penetration of hardened steel plates" (Middle East Technical University, 2010) p.17-22.
60. A. Serjouei, G. Gour, X. Zhang, S. Idapalapati, and G. E. B. Tan, Int. J. Impact Eng. 105 (2017) 54-67.